Technologies and Materials for Renewable Energy, Environment & Sustainability

Superior Hydrogen Energy Conversion Efficiency by UV Visible Light-Driven Efficient TOC Removal in Refinery Wastewater

AIPCP25-CF-TMREES2025-00023 | Article

Superior Hydrogen Energy Conversion Efficiency by UV Visible Light-Driven Efficient TOC Removal in Refinery Wastewater

Nibras N. Mahmood[1, a)] and Mohamed K. Dhahir[1, b)]

[1]*Institute of Laser for Postgraduate Studies, University of Baghdad, Al-Jadriya, Baghdad, Iraq.*

[a)] *Corresponding author: nebras.mahmoud1001@ilps.uobaghdad.edu.iq*
[b)]*mohammed@ilps.uobaghdad.edu.iq*

Abstract. The generation of hydrogen (H_2) by semiconductor-based photocatalysis is seen as cost-effective and environmentally advantageous. This research aimed to produce hydrogen (H_2) while removing contaminants from wastewater by photocatalytic oxidation augmented by laser stimulation, concentrating on the creation of two photoanodes for total organic carbon (TOC) reduction. The exploitation of the band gap between two substrates to improve the absorption of rutile TiO_2/α-Fe_2O_3 photocatalysts in the UV and visible spectra resulted in a significant enhancement in TOC removal rates, reaching 96%. The hydrogen generation rate was 7960 μmol/L, and the solar-to-hydrogen (STH) efficiency was 86.92%, under optimal conditions of pH 3, 40C°, 50 minutes, and a catalyst dosage of 0.4 mg/Lcm², illuminated by a combination of (473+532+632) nm laser and UV source. This study illustrates that rutile TiO_2/α-Fe_2O_3 serve as novel photoanodes for effective (TOC) removal in refinery wastewater and green hydrogen production, representing the most environmentally sustainable option.

K**eywords:** Laser, Wastewater, Pollutant, Photoanodes, Green hydrogen.

INTRODUCTION

Increasing global concerns about environmental deterioration and energy challenges are driving a transition to hydrogen (H_2) as a clean and efficient energy carrier [1]. Hydrogen, a prospective alternative to fossil fuels, offers a solution to the challenges associated with current energy sources, including their environmental impacts and potential health risks [2].

The issues associated with existing hydrogen generation techniques, particularly concerning safety, energy consumption, environmental repercussions, and technical challenges, have hindered their widespread adoption and market success. The combination of these factors limits the feasibility of relying heavily on current hydrogen-generating techniques [3,4]. Photoelectrochemical (PEC) technology, an environmentally benign photooxidation method, provides a sustainable solution for solar energy use and has been extensively employed for the treatment of persistent organic pollutants in wastewater [5]. In the PEC system, the photoanode functions as a vital element, absorbing photons to produce electron-hole (e^--h^+) pairs [6].

The produced H^+ can be directed to the photoanode/electrolyte interface, where it subsequently engages in oxidation reactions [7]. The essential elements for constructing a highly efficient PEC system comprise the development of a robust photoanode [8]. That facilitates effective charge separation, rapid charge transfers kinetics, and swift surface chemical reactions [9]. Various semiconductor materials, including WO_3, TiO_2, α-Fe_2O_3, BiOI, and $BiVO_4$, have been employed as photoanodes in PEC systems [11].

To improve the effectiveness of photoelectrocatalysis for hydrogen production. It is essential to select the optimal light intensity according to the specific characteristics and reaction conditions, [12] of the process to maximize photo-generated charge yield and hydrogen production efficiency, as well as to choose the appropriate spectral range utilizing optical filters [13,14]. This research examines the efficacy of rutile TiO_2/α-Fe_2O_3 as a photoanode. The study demonstrates the effectiveness of charge separation and transfer between rutile TiO_2 and α-Fe_2O_3. The material exhibits profound absorption of visible light and a negligible recombination rate of electron-hole pairs. An augmented specific surface area provides a higher quantity of active sites for photocatalytic reactions. As a result, the photo-

induced charge carriers can more easily migrate to the surface to break down the adsorbed organics for refinery wastewater treatment.
Despite the significant benefits, to our knowledge, no studies have been conducted on the utilization of rutile TiO_2/α-Fe_2O_3 nanocomposites for total organic carbon treatment in refinery effluent and hydrogen generation.

CHARACTERISTICS OF PETROLEUM REFINERY EFFLUENTS

This research utilized ten liters of effluent sourced from the Al-Dora petroleum refinery in Iraq. The PRW sample was collected from the tank before the biological treatment unit. The sample was preserved at 4 C° in a laboratory refrigerator until employed. Total Organic Carbon (TOC) was measured using the LANGE device (S/N 1485515, Germany), while the pH, Electrical Conductivity (EC), Total Dissolved Solids (TDS), and temperature of the electrolyte were evaluated with the TK303PLUS Water Quality Meter (Suzhou Holi Smart Technology Co., Ltd, China). Table (1) outlines the characteristics of samples analyzed before the experiments to determine their chemical and physical properties.

TABLE 1. Illustrates The Properties of Samples

Parameter	Value
pH	8.5
Temperature C°	25
TOC (ppm)	14.6
Total Dissolved Solid (ppm)	554
Conductivity (µS/cm)	1024

EXPERIMENTAL METHODS

Materials

Deionized (DI) water was employed as the solvent for all concentrations. Titanium dioxide (TiO_2-Rutile) nanopowder, exhibiting a purity of 99.9%, was procured from US Research Nanomaterials, Inc. (USA). α-Fe_2O_3 iron oxide nanopowder, with a purity of 99.9%, was acquired from the same provider. The pH of the refinery effluent was modified by incorporating quantified quantities of H_2SO_4 and NaOH obtained from Scharlau, Spain.

Fabrication of the Rutile TiO_2/ α- Fe_2O_3 Photoanode

The photoanode is a thin film coated with fluorine-doped tin oxide, rutile titanium dioxide, and alpha-iron oxide nanoparticles. A total of 0.399 g of rutile TiO_2 nanoparticles was dispersed in 25 mL of deionized water. The mixture was magnetically stirred for one hour at room temperature to ensure proper dispersion of the TiO_2 nanoparticles. The second layer was formed by dispersing 0.798 g of rutile α-Fe_2O_3 nanoparticles in 25 mL of deionized water. This layer was applied to a 1 x 1 cm section of the FTO substrate, which measures 1 × 2 cm. Subsequently, the film was allowed to cure on a heated surface. A micropipette was used for drop-casting the subsequent concentration of the rutile TiO_2/α-Fe_2O_3 catalyst, measuring 0.4 mg/L cm^2.

MATERIALS CHARACTERIZATIONS

X-Ray Diffraction Measurement (XRD)

XRD (X-ray diffraction) was utilized to examine the structural characteristics of TiO_2 nanoparticles and α-Fe_2O_3 nanoparticles with an Aeris X-ray diffractometer. The scanning range was established between 20° and 80°, with a peak location accuracy of ± 0.02°, as depicted in Fig. (1). The detected peaks correspond with the standard indicated in JCPDS Card No. 21-1276 [15,16].

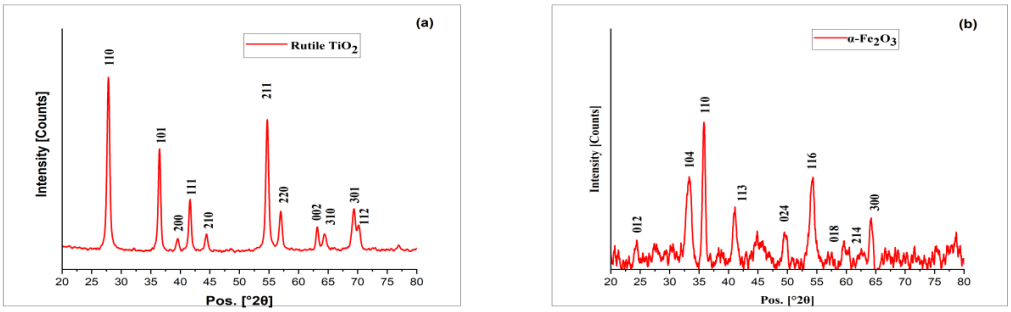

FIGURE 1. XRD Pattern. (a) rutile TiO_2 (NP) (b) α-Fe_2O_3 (NP)

Fig. (1) shows X-ray diffraction (XRD) patterns of α-Fe_2O_3 nanoparticles, with characteristic lines corresponding to diffraction peaks. This is comparable to the (JCPDS Card No. 86–0550) [17,18].

Field Emission Scanning Electron Microscopy (FESEM)

The relatively high surface area of TiO_2 (NP) and α-Fe_2O_3 (NP) is attributed to the nanostructured surfaces of the particles, as confirmed by the FESEM analysis in Fig. (2). The large surface area is crucial in specific applications, such as photocatalysis, where absorption is fundamental in the PEC cell [19, 20].

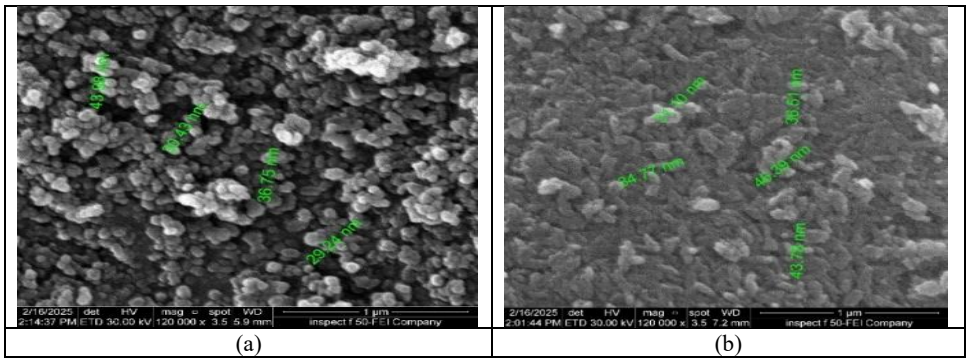

FIGURE 2. FESEM (a) Rutile TiO_2 (NP). (b) α- Fe_2O_3 (NP).

Optical Analysis

The UV-VIS-NIR -1800 (SHIMADZU, Japan) spectrophotometer was utilized to analyze the optical properties of the photoanode. This apparatus was digitized utilizing a CRT display and a keypad for input value manipulation The absorption spectra were mapped across a wavelength range of 190 to 1100 nm. The optical properties and band alignment of the photoelectrode are crucial for improving photoelectrochemical (PEC) performance. The band gap energy (Ebg) of the thin film was ascertained utilizing the the absorption data of the photo anode, in comparison to a thin film produced simply with the initial layer of TiO_2 nanoparticles, to highlight the shift in band gap following the incorporation of additional material layers. Utilizing Tauc's equation:

$$\alpha h\nu = A(h\nu - Ebg)^n \quad (1)$$

where α is the absorption coefficient, h is Planck's constant, v is the photon frequency, A is the probability parameter for the transition, Ebg is the optical bandgap, and n is the type of transition [19,20]. the band gap value diminished for the first and final photoanodes from 3.03 eV to 2.71 eV. Substantially reduced the band gap, resulting in improved absorption activity in the visible spectrum from 400 to 700 nm and near-infrared at 856 nm, as illustrated in Fig. (3). which enhanced the performance of the PEC cell for hydrogen production.

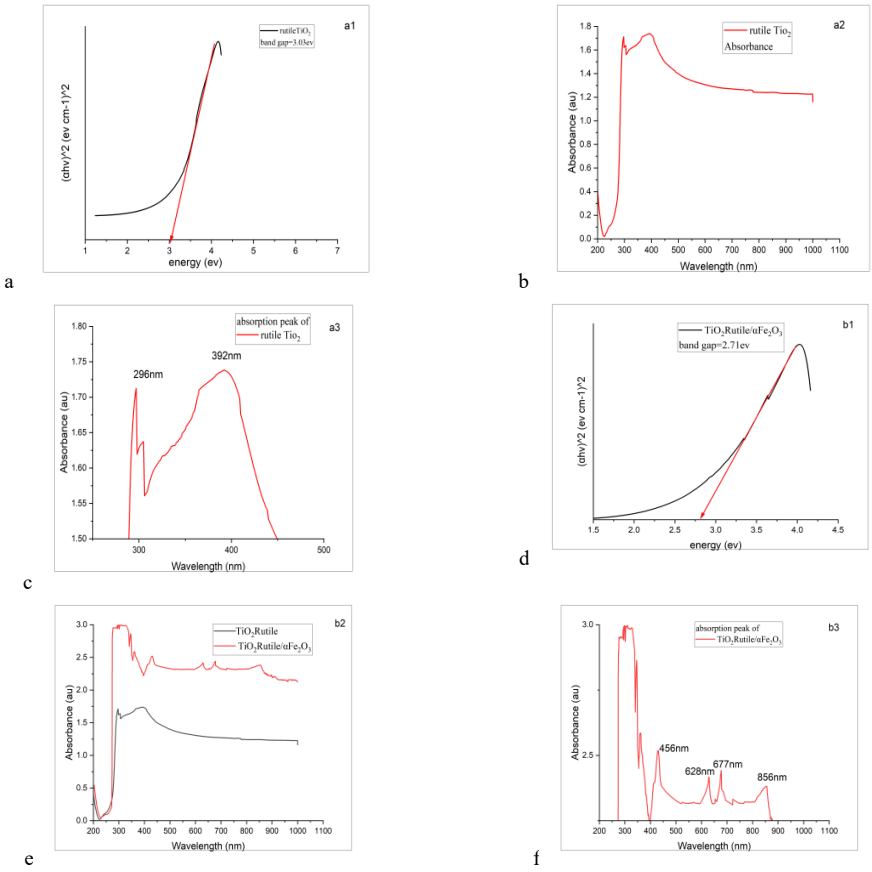

FIGURE 3a,b,c,d,e,f. Band Gap and Absorbance Spectrum (a)Rutile TiO_2 (b) Rutile TiO_2/ α- Fe_2O_3

Photo Electrochemical Characteristics

The photoelectrochemical properties were assessed utilizing an electrochemical workstation (ER466, EDAQ Company, Australia, potentiostat). In this configuration, Ag/AgCl acted as the reference electrode, whereas Pt served as the counter electrode. The two specified photoanodes, rutile TiO_2 and rutile TiO_2/α-Fe_2O_3, functioned as the working electrodes in a three-electrode configuration. Routine testing was performed at ambient temperature using a 125 mL quartz cuvette. The pH of the refinery wastewater was modified by the addition of precise quantities of 0.5 mg H_2SO_4 and NaOH, which served as the electrolyte. The linear sweep voltammetry curve was acquired by scanning from 0 to 5 V relative to Ag/AgCl. J-V curves were obtained at a rate of 100 mW/s and a frequency of 20 kHz throughout the experimental program. The wastewater and catalyst were agitated continuously at 50 rpm in darkness for 30 minutes to improve physical absorption. The reactor's efficiency was enhanced by continuous upward mixing enabled by a pump. The reaction was subsequently subjected to a 6 W ultraviolet source generating light at approximately 290 nm, in conjunction with three visible lasers: a blue laser operating at 473 nm and 200 mW, a green laser at 532 nm and 100 mW, and a red laser at 632 nm and 132 mW. The illumination was administered to the photoanode at AM 1.5 G conditions at 100 mW/cm². The solar standard state of illumination was attained utilizing an attenuator, as depicted in Fig. (4), which demonstrates the experimental methodologies.

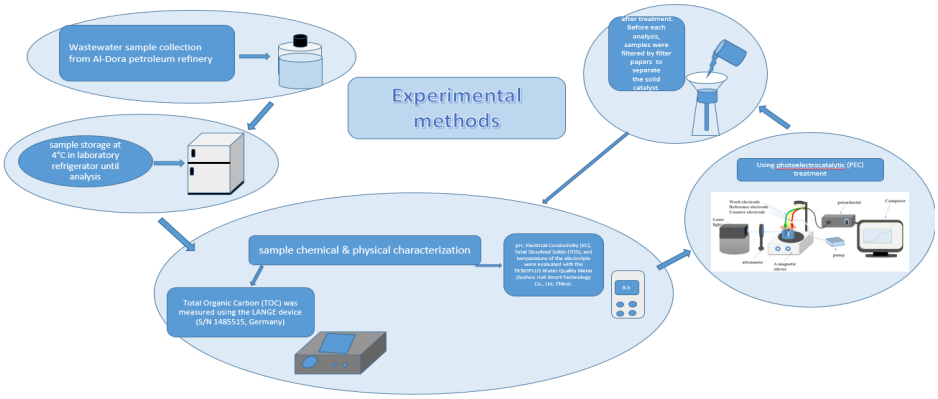

FIGURE 4. Schematic of Experimental Methods.

The efficacy of TOC removal was assessed utilizing equation (2).

$$RE = \frac{C_o - C_t}{C_o} \times 100\% \quad (2)$$

where C_t signifies the concentration at a given moment and C_o indicates the initial concentration. RE% signifies removal efficiency [21].

The Experimental Performances

The comprehensive assessment of photoanode performance commences with the examination of dark current, which signifies the baseline current in the absence of light exposure. We affirm that the incident light only produces the documented photocurrent, guaranteeing its immunity to extraneous factors, and we strive for accurate assessments of PEC performance. The synthesized photoanodes, rutile TiO_2 and rutile TiO_2/α-Fe_2O_3, were assessed, as seen in Fig. 5, utilizing voltage scans from 0 to 5 V relative to Ag/AgCl in the absence of light. The dark current density of the rutile TiO_2 working electrode rose from 10 to 14 $mA \cdot cm^{-2}$ following the incorporation of α-Fe_2O_3 (NP) as a secondary layer in the thin film manufacturing. This rise corresponds with an improvement in conductivity.

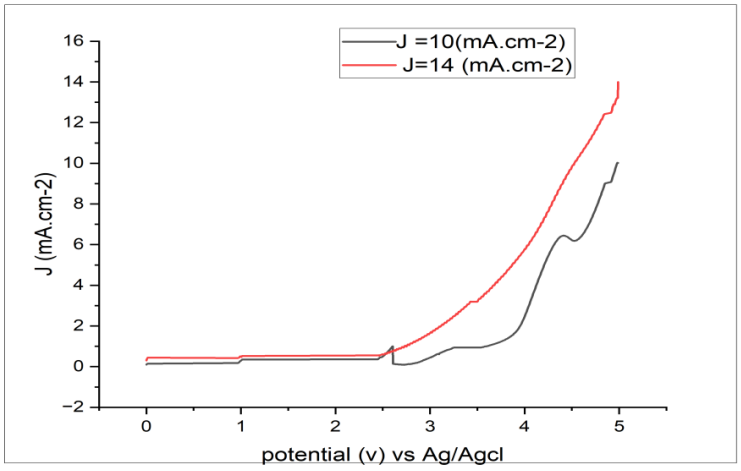

FIGURE 5. Dark Current I-V Curve Tested by Linear Sweep Voltammetry.

Photo-Catalysis Process

Previous studies have comprehensively studied the application of photo-catalysis for Hydrogen production in wastewater treatment. Table 2 delineates the principal publications together with their operational parameters and photocatalytic type.

TABLE 2. Evaluation of Photocatalytic Efficacy for Hydrogen Production from Wastewater

Photocatalys type	Light source	Wastewater	Hydrogen Production	Year and Reference
Methyl Orange (azo dye) wastewater	UV light	Aqueous with cellulose (sacrificial biomass)	1216 μmol/L	Vaiano, V. et al., 2019 Ref. [22]
Pt–TiO_2–Nb_2O_5	UV light	Aqueous glycerol solution	6657 μmol/L	Iervolino, G., et al., 2021 Ref. [23]
ZnOSAS/1%RuO_2SAS	UV light	Gallic acid (GA) solution	4461 μmol/L	Iervolino, G. et al., 2025 Ref.[24]
rutile TiO_2/ α- Fe_2O_3	UV-visible light	Refinery wastewater	7960 μmol/L	This study

RESULTS AND DISCUSSION

Photo-Electrochemical Behavior of Photoanode Under Illumination

The J-V curves were acquired during a scan commencing at 0-5 V vs Ag/AgCl under AM 1.5 G illumination at a power density of 100 mW/cm². A comparison method was utilized to attain the most precise assessment of the photoelectric response of the fabricated photoanodes. In a photoelectrochemical (PEC) system, the photoanode is an essential element that absorbs photons to produce electron-hole (e^--h^+) pairs. The produced H^+ ions can be directed to the interface between the photoanode and the electrolyte [25]. The photo-generated electrons and holes finally transform hydrogen ions into hydrogen molecules via processes involving the photo-generated electrons. The efficiency of H_2 production in this process will markedly enhance with a greater surface area of the material system, offering abundant active sites for chemical reactions, and exhibiting superior carrier conductivity, which accelerates chemical processes. As a result, the rutile TiO_2/α-Fe_2O_3 nanocomposites, distinguished by elevated porosity and conductivity, exhibit an enhanced H_2 generation rate, especially in comparison to rutile TiO_2.

Effect of Laser Wavelength

Photocatalytic experiments utilized three varieties of visible lasers: a blue laser at 473 nm and 200 mW, a green laser at 532 nm and 100 mW, and a red laser at 632 nm and 132 mW. A UV source emitting roughly 290 nm at 6 W illuminated the photoanode at AM 1.5 G conditions at 100 mW/cm². The evaluation of photoactivity was conducted under ideal conditions, namely at a temperature of 40°C, pH 3, a reaction length of 50 minutes, and a catalyst dosage of 0.4 mg/lcm², employing two photoanodes: rutile TiO_2 and rutile TiO_2/α-Fe_2O_3 for the degradation of total organic carbon in refinery effluent. The findings are depicted in Figures 6 and 10. The experiments indicated a TOC removal rate of 59.75% and a hydrogen production rate of 2320.8 μmol/L at a current density of 30 mA/cm² utilizing a UV source. The rutile TiO_2/α-Fe_2O_3 photocatalyst attained a removal efficiency of 68% and a hydrogen production rate of 2908 μmol/L at a current density of 33 mA/cm² under red visible laser irradiation. In contrast, the rutile TiO_2/α-Fe_2O_3 catalyst demonstrated removal rates of 80.55%, a current density of 40 mA/cm², and a hydrogen generation rate of 4175 μmol/L under illumination from a green visible laser. A 93% removal efficiency was observed for rutile TiO_2/α-Fe_2O_3 when subjected to a blue visible laser, with a current density of 57.34 mA/cm² and an increased hydrogen generation rate of 6920.8 μmol/L. As a result, an elimination efficiency of 93.2% and a hydrogen production rate of 7,183 μmol/L were attained using three visible lasers at a current density of 59 mA/cm². The utilization of the rutile TiO_2/α-Fe_2O_3 photocatalyst under UV and three visible light sources resulted in a notable enhancement in TOC removal rates to 96% and a hydrogen production rate of 7960 μmol/L at a current density of 64 mA/cm². The results are encouraging, as the removal efficiencies under visible light were marginally inferior to those recorded under UV and three visible light conditions. The rutile TiO_2/α-Fe_2O_3 photoanode created in this study exhibited promising outcomes, with visible light facilitating very efficient removal. The intensity of light directly influences the quantity of photogenerated charge and, subsequently, hydrogen generation. As light intensity escalates, the amount of

photogenerated charge grows, consequently augmenting the pace of hydrogen production. Consequently, choosing the ideal light intensity is crucial for enhancing the effectiveness of photoelectrocatalytic hydrogen production.

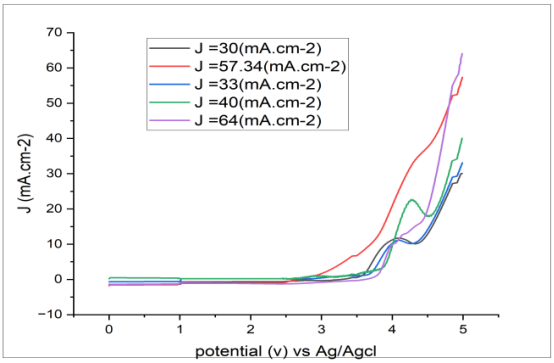

FIGURE 6. Effect of Laser Wavelength on I-V Curve Tested by Linear Sweep Voltammetry.

THE SOLAR TO HYDROGEN EFFICIENCY (η)

The efficiency of solar-to-hydrogen conversion was determined using Equation 3, which involves dividing the product of the H_2 evolution rate and the Gibbs free energy required to produce one mole of H_2 from water by the total power of incident simulated sunlight (AM1.5G) multiplied by the area exposed to the incident light [26].

$$\mathrm{STH}(\%) = \left[\frac{(\mathrm{mmol\ H_2/s})\times(273\mathrm{kJ/mol})}{\mathrm{P_{total}(mW/cm^2)}\times \mathrm{area(cm^2)}}\right] \times 100\% AM1.5G \quad (3)$$

The Solar-to-Hydrogen efficiency of the rutile TiO_2/α-Fe_2O_3 photoanode, illuminated by a combination of (473+532+632) nm lasers and a UV source, is 86.92% far surpassing other reported efficiencies, indicating a robust capacity for hydrogen synthesis. Furthermore, this results in the overall superior performance of the PEC cell. The effectiveness of rutile TiO_2 photoanode is 25.36% under UV illumination. The obtained results are depicted in Fig. 7.

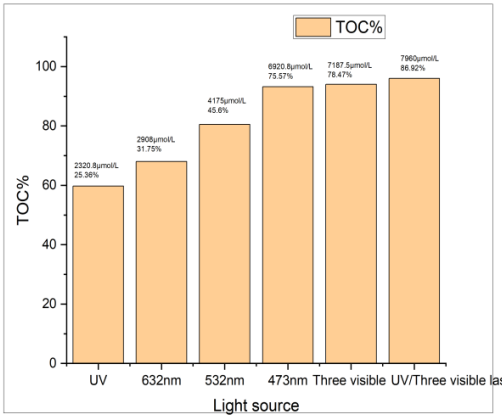

FIGURE 7. Effect of Laser Wavelength on TOC Degradation and Hydrogen Production

CONCLUSIONS

This investigation revealed that the rutile TiO_2/α-Fe_2O_3 photoanode achieved the highest degradation efficiency in refinery wastewater when exposed to UV light and three visible light sources under AM 1.5 G conditions of 100 mW/cm². The optimal parameters included a pH 3, 40C°, a catalyst dosage of 0.4 mg/Lcm², and 50 minutes. These conditions resulted in a 96% reduction in total organic carbon (TOC) levels, a current density of 64 mA/cm², a

hydrogen generation rate of 7960 μmol/L, and a solar-to-hydrogen conversion efficiency of 86.92%. The enhanced photocatalytic performance of the rutile TiO_2/α-Fe_2O_3 is attributed to improved absorption of UV and visible light, efficient charge-carrier separation, and the synergistic interactions between rutile TiO_2 and α-Fe_2O_3. This study introduces novel application of rutile TiO_2/α-Fe_2O_3 semiconductor composite photocatalyst for tremediation of TOC in refinery effluent.

REFERENCES

1. R. Yang, L. Mei, Y. Fan, Q. Zhang, R. Zhu, et al., Small Methods 5, 2100887 (2021). https://doi.org/10.1016/j.cej.2018.08.028
2. Y. Pan, X. Yuan, L. Jiang, H. Yu, J. Zhang, H. Wang, R. Guan, G. Zeng, Chem. Eng. J. 354, 407 (2018). https://doi.org/10.1016/j.cej.2018.08.028
3. Ibrahim, H.M. and Salman, R.H., 2022. Real wastewater treatment by electrocoagulation-electro-oxidation combined system: Optimization using Taguchi approach. Egyptian Journal of Chemistry, 65(3), pp.135-145. https://doi.org/10.21608/ejchem.2021.88245.4247
4. Al-Ani, S.A. and Dhahir, M.K., 2025. Enhance the efficiency of [CeO2 (NP)/Cu (NP)] PEC cell photoanode for hydrogen production by laser illumination. Iraqi Journal of Laser, 24(1), pp.21-30. https://doi.org/10.31900/ijl.v24i1.499
5. G. Zhang, H. Wu, D. Chen, N. Li, Q. Xu, H. Li, J. He, J. Lu, Green Energy Environ. 7, 176 (2022). https://doi.org/10.1016/j.gee.2020.12.015
6. M. Tang, W. Yin, F. Zhang, X. Liu, L. Wang, Front. Chem. 10, 959414 (2022).
7. Al-Ani, S.A. and Dhahir, M.K., 2025. Effect of Ideal Thickness on Boosting Efficiency of Photoelectrochemical Cell Photoanode via Maximal Absorption. Iraqi Journal of Applied Physics, 21(1), pp.17-26.
8. Ibrahim, H.M., 2022. Study the optimization of petroleum refinery wastewater treatment by successive electrocoagulation and electro-oxidation systems. Iraqi Journal of Chemical and Petroleum Engineering, 23(1), pp.31-41. https://doi.org/10.31699/IJCPE.2022.1.5.
9. L. Yao, S. Zeng, S. Yang, H. Zhang, Y. Ma, G. Zhou, J. Fang, Catalysts 15, 271 (2025). https://doi.org/10.3390/catal15030271
10. Al-Ani, S.A. and Dhahir, M.K., 2024. Laser-Enhanced Hydrogen Production: Designing a PEC Cell Photoanode with an Exclusive Dye Material for Superior Efficiency. Renewable Energy & Sustainable Development, 10(2). https://doi.org/10.21622/RESD.2024.10.2.1050
11. Y. Qin, H. Li, J. Lu, et al., Appl. Catal. B 277, 119254 (2020). https://doi.org/10.1016/j.apcatb.2020.119254
12. Khalaf, H.T. and Faris, R.A., 2025. Enhanced photocatalytic degradation of methylene blue using MWCNTs. Results in Optics, 18, p.100776. https://doi.org/10.1016/j.rio.2025.100776.
13. S. Li, G. Zhang, D. Meng, F. Yang, Chem. Eng. J. 485, 149828 (2024). https://doi.org/10.1016/j.cej.2024.149828
14. S. Palmas, L. Mais, M. Mascia, A. Vacca, Curr. Opin. Electrochem. 28, 100699 (2021). https://doi.org/10.1016/j.coelec.2021.100699
15. P. Santos-Aguilar, J. Bernal-Ramírez, E. Vázquez-Garza, L. Y. Vélez-Escamilla, O. Lozano, G. D. J. García-Rivas, ACS Omega 8, 19024 (2023). https://doi.org/10.1021/acsomega.3c01747
16. M. S. Hossain, S. Ahmed, Results Mater. 20, 100492 (2023). https://doi.org/10.1016/j.rinma.2023.100492.
17. J. Electroceram. 45, 7 (2020). https://doi.org/10.1007/s10832-020-00366-3
18. G. H. Jihad, Iraqi J. Sci. 62, 3901 (2021). https://doi.org/10.24996/ijs.2021.62.11.11
19. T. Charitha, U. Leshan, M. Shanitha, W. Ramanee, L. Buddi, and B. Martin, Results Mater. 12, 100219 (2021). https://doi.org/10.1016/j.rinma.2021.100219

A. A. Ayachi, H. Mechakra, M. M. Silvan, S. Boudjaadar, S. Achour, Ceram. Int. 41, 2228 (2015). https://doi.org/10.1016/j.ceramint.2014.09.163

20. L. Usgodaarachchi, C. Thambiliyagodage, R. Wijesekera, S. Vigneswaran, M. Kandanapitiye, ACS Omega 7, 27617 (2022). https://doi.org/10.1021/acsomega.2c03848
21. X. Zhang, L. Luo, R. Yun, M. Pu, B. Zhang, X. Xiang, ACS Sustain. Chem. Eng. 7, 13856 (2019). https://doi.org/10.1021/acssuschemeng.9b03219
22. M. Kumar, N. K. Singh, R. S. Kumar, R. Singh, in Towards Sustainable and Green Hydrogen Production by Photocatalysis: Insights into Design and Development of Efficient Materials, Vol. 2 (ACS, 2024), pp. 1–24.
23. G. Iervolino, C. Falchetta, S. Mottola, I. De Marco, V. Vaiano, Fuel 388, 134480 (2025).
24. Y. Li, B. Bai, M. Zhu, J. Li, Q. Mei, Q. Wang, J. Environ. Chem. Eng. 12, 113079 (2024).
25. N. L. De Silva, A. C. A. Jayasundera, A. Folger, O. Kasian, S. Zhang, C.-F. Yan, C. Scheu, and J. Bandara, Catal. Sci. Technol. 8, 4657 (2018). https://doi.org/10.1039/C8CY01212A